

Article

Characterization and Dynamic Adjustment of the Flow Field during the Late Stage of Waterflooding in Strongly Heterogeneous Reservoirs

Daigang Wang ^{1,*} , Fangzhou Liu ¹, Guoyong Li ^{2,*}, Shumei He ³, Kaoping Song ¹ and Jing Zhang ^{4,*}

¹ State Key Laboratory of Petroleum Resources and Prospecting, China University of Petroleum, Beijing 102249, China; 2020211839@student.cup.edu.cn (F.L.); skpskp01@sina.com (K.S.)

² Jidong Oilfield of CNPC, Tangshan 063200, China

³ Petro China Da Gang Oilfield Exploration and Development Research Institute, Tianjin 300280, China; heshmei@petrochina.com.cn

⁴ Research Institute of Petroleum Exploration and Development, PetroChina, Beijing 100083, China

* Correspondence: dgwang@cup.edu.cn (D.W.); jd_lgy@petrochina.com.cn (G.L.); zing@petrochina.com.cn (J.Z.)

Abstract: The flow field is the fluid dynamic flow path in strongly heterogeneous reservoirs, and its evolution significantly affects the distribution of remaining oil, showing a disordered and highly dispersed mode caused by long-time water injection. By combining traditional flow-field evaluation with flow diagnostics, this paper proposes a methodology to quantitatively characterize and adjust the flow field in real time during the late stage of waterflooding in strongly heterogeneous reservoirs. In the study, the fluid velocity, abundance of predominant remaining oil, and Lorenz coefficient are preferred as the characteristic parameters to evaluate the effect of reservoir and flow heterogeneity on the flow field. Taking the minimization of the Lorenz coefficient as the objective function, the optimal injection and production parameters are obtained by dynamic adjusting the flow field. The results show that as water injection continues, the shape and variation of the flow field are jointly influenced by the reservoir rhythm, vertical permeability contrast, and lateral permeability distribution. The larger the permeability contrast, the greater the influence of the lateral permeability distribution. When the permeability contrast is large, the Lorenz coefficient strongly depends on the lateral permeability distribution. Finally, this method is applied to an actual heterogeneous reservoir, and a better effect of oil increase and water reduction is achieved.

Keywords: waterflooding; reservoir heterogeneity; flow field; potential tapping; remaining oil



Citation: Wang, D.; Liu, F.; Li, G.; He, S.; Song, K.; Zhang, J.

Characterization and Dynamic Adjustment of the Flow Field during the Late Stage of Waterflooding in Strongly Heterogeneous Reservoirs.

Energies **2023**, *16*, 831. <https://doi.org/10.3390/en16020831>

Academic Editor: Rouhi Farajzadeh

Received: 7 December 2022

Revised: 28 December 2022

Accepted: 7 January 2023

Published: 11 January 2023



Copyright: © 2023 by the authors. Licensee MDPI, Basel, Switzerland. This article is an open access article distributed under the terms and conditions of the Creative Commons Attribution (CC BY) license (<https://creativecommons.org/licenses/by/4.0/>).

1. Introduction

Most of the developed reservoirs in China belong to continental deposits with serious lateral and vertical heterogeneities. After extensive water injection, most of oil fields have come into a high or extra-high water-cut period, and the remaining oil is strongly disordered, showing an overall highly dispersed and relatively enriched local distribution. It is a great challenge during the late stage of waterflooding to describe the remaining oil distribution and determine reasonable strategies to further improve oil recovery. The flow field is the dynamic flow path of reservoir fluids, and its evolution significantly affects the distribution of remaining oil. The evolution of the flow field is very complicated, affected by the geological conditions, well pattern, and fluid properties. In some areas, it tends to form a dominant flow field due to excessive water injection. The uneven distribution of the flow field typically leads to a highly scattered distribution of remaining oil and severe ineffective water circulation. Accurate description of the fluid flow field in reservoirs is of great significance to understand the underlying dynamics of multiphase flow, optimize the well pattern, and enhance oil recovery.

During water flooding, fast movement of the waterfront is usually caused by tectonic fractures, faults, and lateral permeability distribution, which indicates ineffective water circulation, low sweep efficiency and oil recovery. Extensive water injection will affect the rock pore structure and mineral composition, causing obvious variations in reservoir properties, e.g., porosity, permeability, and wettability [1]. Jiang et al. concluded that the variation of reservoir properties is typically proportional to the cumulative injected pore volume of water, which is more distinct during the high or extra-high water-cut period [2]. In-depth study of fluid flow paths is beneficial to accurately describe the flow field during the late stage of waterflooding in strongly heterogeneous reservoirs. Flow-diagnostics tools can be utilized to efficiently characterize the reservoir connectivity and dynamic evolution of the fluid flow path [3–6]. In contrast to the full-physics simulation, flow diagnostics have the advantages of a fast calculation speed, high calculation efficiency, and low model complexity. As a popular technique, streamline-based simulation [7–13] is widely used to estimate parameters such as the time of flight and steady-state tracer distribution. Moreover, great efforts have been made to describe the flow heterogeneity and several characteristic properties are then proposed, such as the sweep region, drainage region, well-pair region, and Lorenz coefficient, which are helpful to describe the fluid flow dynamics in a reservoir. Thiele and Batycky employed streamline-based simulation to calculate the flux between well pairs and obtained the optimal injection-production parameters [10]. Jia and Deng developed a flow-field identification method based on streamline simulation [14]. By Python programming, streamline clusters are analyzed to identify the ineffective water circulation region. Tanaka et al. combined streamline-based simulation and genetic algorithm to obtain the preliminary development schemes [15]. The response surface is then coupled to achieve the optimal scheme of a typical waterflooding reservoir, which can reduce the model complexity to a great extent.

Previous studies showed that the streamline-based models with a hexahedral grid are computationally efficient, but the computational efficiency decreases significantly when extended to more complex unstructured grids. The finite volume method was typically utilized to simulate fluid flow on structured and unstructured grids to calculate the time of flight and tracer distribution. Some scholars presented a family of implicit discontinuous Galerkin schemes for advective multiphase flow simulation in porous media, which are more suitable for complex grids and more accurate than streamline-based simulation [16–19]. Shahvali et al. also solved the time of flight and tracer distribution equations using the finite volume method [20]. To avoid numerical diffusion, a multi-dimensional weighting method was introduced to solve the steady transport equation. The results were then compared with those of streamline-based simulation to validate the method. Møyner et al. extended the method to corner-point grids and then used the finite volume method to solve the incompressible fluid pressure equations [21]. Zhang et al. further developed a control-volume finite element method to solve hyperbolic transport equations for the time of flight and tracer distribution [22]. To improve the computational efficiency, Rasmussen and Lie introduced two methods for numerical discretization, a multi-dimensional upwind method and a higher-order discontinuous Galerkin method [23]. Except for flow diagnostics, the flow-field strength is also used to describe the flow field; Zhang et al. presented surface flux as a flow-field-evaluation index and further established a relationship between the flow-field strength and oil saturation [24]. Jiang et al. also utilized the surface flux to evaluate the flow field [25].

Flow diagnostics tools can also be utilized to optimize the injection-production parameters. Compared with the traditional full-physics simulation method, flow diagnostics tools show considerable improvement in computational efficiency. However, the flow diagnostics tools are mainly used to describe the overall state of fluid flow in a reservoir. Full-physics simulation is preferred to understand the local flow state and explain the effect of reservoir heterogeneity on the flow state. Research on the evolution of the flow field affected simultaneously by flow heterogeneity and reservoir heterogeneity is still insufficient, and it is more difficult to exploit the remaining oil potential during the high or

extra-high water-cut period. Moreover, when the reservoir geological model is complex, the selection of an optimization scheme requires a lot of computing resources. To solve the above problems, we combine the full-physics simulation and flow diagnosis to describe the flow field, and distinguish the flow regions with different capabilities of waterflooding. We aim to establish a novel characterization and adjustment method of the flow field in the late stage of a waterflooding reservoir with strong heterogeneity. This method can reproduce the historical state of subsurface fluid and put forward more targeted adjustment strategies for oilfield development.

The structure of this article is as follows: (1) the flow characterization of the flow field is performed by estimation of the flow-field strength and flow diagnostics; (2) the dynamic evolution of the flow field affected simultaneously by flow heterogeneity and reservoir heterogeneity is further discussed; (3) taking the Lorenz coefficient minimization as the objective function, a dynamic adjustment method of the flow field is developed; (4) finally, the proposed methodology is applied to study the fluid-flow behavior, analyze the spatial distribution of the remaining oil, and achieve optimal injection-production parameters for a typical continental sandstone reservoir with strong heterogeneity.

2. Flow-Field Characterization of Waterflooding Reservoir

The flow field is a complex system with multiple factors interacting with each other. Various dynamic and static properties should be considered to evaluate the flow field. The widely used static parameters consist of porosity, permeability, effective thickness, etc., while dynamic factors typically denote the fluid pressure, saturation, and flow velocity. The existing methods mainly map the grid attributes to the flow field without considering the dynamic variation of the reservoir flow path. Combining grid attribute mapping with flow path characterization, the dynamic evolution of the flow field considering the influence of reservoir heterogeneity and flow heterogeneity is explored here. The flow field properties and flow heterogeneity are realized through MATLAB programming, and the calculation process will be described in this chapter.

2.1. Grid Attribute Mapping-Based Flow Field Properties

The dynamic properties of reservoir flow field evaluation can be categorized into adjustment and displacement parameters. The adjustment properties typically include the fluid pressure, fluid velocity, etc. These properties can be used to understand the instantaneous behavior of the reservoir flow field by describing the adjustment ability of injection and production. The displacement parameters typically consist of the pore volume of water injected, water saturation, and oil saturation, mainly reflecting the cumulative variation of the reservoir flow field over time.

In this study, the fluid velocity is first selected as one of the adjustment properties. Fluid velocity refers to the fluid flow capacity per unit time and cross-section, which can be regarded as a local indicator reflecting the relative variation of velocity between grids without considering the change in fluid velocity along a certain flow path. Due to the gradually increasing resistance along the flow path, there may be a situation in which the local velocity is low but the velocity along a certain flow path is high. Therefore, the fluid velocity has some inherent limitations regarding its ability to characterize the actual flow field.

The abundance of remaining reserves is typically treated as a displacement parameter of the reservoir flow field. The abundance of remaining reserves refers to the geological reserves of the remaining oil per unit area, which characterizes the influence of multiple parameters such as the effective thickness, porosity, oil saturation, and fluid properties but cannot accurately reflect the complicated fluid distribution of oil and water in a reservoir during a high or extra-high water-cut period. Geng et al. introduced the abundance of the predominant remaining oil to characterize the dominant distribution of remaining oil at a

high water-cut stage [26]. The parameter couples the abundance of remaining oil reserves and the diversion capacity of the remaining oil, which can be expressed as:

$$\Omega = \frac{100A_3h\varphi\rho_o}{B_o}, \quad (1)$$

$$A_3 = \frac{K_{ro}\mu_w}{K_{rw}\mu_o}S_o, \quad (2)$$

where Ω is the abundance of the predominant remaining oil; A_3 is the diversion capacity coefficient; μ_w is the water viscosity, mPa s; and μ_o is the oil density, mPa s.

For this study, the fluid velocity and abundance of the predominant remaining oil are screened to classify and evaluate the reservoir flow field. Because of the difference in units and orders of magnitude of these two indicators, two parameters are first converted into [0, 1] for further analysis. The instantaneous behavior of the flow field and cumulative effect after a long period of water injection are analyzed.

2.2. Evaluation of Flow Heterogeneity

Time of flight was widely used to characterize the reservoir flow heterogeneity [27]. The characteristic parameters of the flow field, Lorenz curve, and Lorenz coefficient can be estimated using the time of flight.

Tracer dynamic monitoring technology has been used to trace injected water by means of adding a mixture tracer into the water injector. It can give information by monitoring the water flow velocity, direction, path, and other properties. Time of flight can be calculated in a similar way to the tracer dynamic monitoring technology, where the time of flight is the time required for a neutral particle to move from the nearest source or inflow boundary to a certain point in the reservoir. The time of flight includes the forward time of flight and backward time of flight. The forward time of flight is the time required for a tracer injected at the source or inflow boundary to reach a specific location of a reservoir, reflecting the sweep volume of the injected fluid. The backward time of flight is the time required for a tracer released at a given location in a reservoir to reach the source or inflow boundary, reflecting the sweep volume of the producer [28,29]. The time of flight is generally calculated using the finite volume method [30], which can be calculated as follows:

$$-\vec{v} \times \nabla \tau_b = \varphi, \tau_b \Big|_{outflow} = 0, \quad (3)$$

$$-\vec{v} \times \nabla \tau_f = \varphi, \tau_f \Big|_{outflow} = 0, \quad (4)$$

where φ is the porosity; \vec{v} is the velocity, m/s; τ_f is the forward time of flight; and τ_b is the backward time of flight.

By adding the forward time of flight and the backward time of flight, the total time of flight will be obtained. It reflects the dynamic variation of fluid movement over time, which can explain more details of the flow field. Areas with longer flight times usually show a lower sweep volume and more remaining oil.

The Lorenz curve was originally proposed to characterize reservoir heterogeneity and inequality in the vertical water injection and production profile [31]. Shook and Mitchell extended the traditional Lorenz curve to flow heterogeneity and introduced the storage-capacity–flow-capacity graph and Lorenz coefficient to characterize flow heterogeneity [32]. The storage capacity is the pore volume as a function of the time of flight, and the flow capacity is the cumulative flow under a specific time interval. To eliminate the effect of the magnitude, the storage capacity and flow capacity need to be normalized. The storage capacity is chosen as X coordinate and the flow capacity as Y coordinate to plot the Lorenz curve. In general, the Lorenz curve is used to evaluate the degree of flow heterogeneity. The closer the curve is to a straight line, the weaker the flow heterogeneity is, and the better the displacement efficiency is. For one-dimensional displacement, the Lorenz curve shows

the variation of fractional flow with saturation, and when the case is homogeneous, the curve will be a straight line, as shown in Figure 1.

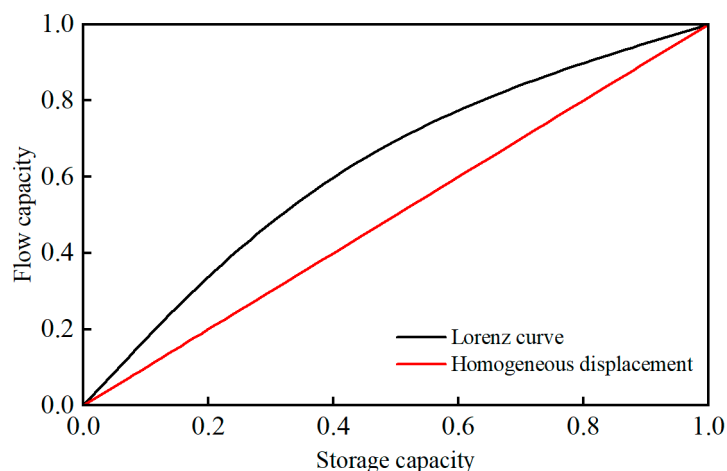


Figure 1. Typical storage-capacity–flow-capacity Lorenz curve.

Once the Lorenz curve is plotted, the Lorenz coefficient can be computed by integration, and the expression is described as:

$$L_c = 2 \int_0^1 [F(\Phi) - \Phi] d\Phi, \tag{5}$$

The Lorenz coefficient is a decimal between 0 and 1. The smaller the Lorenz coefficient, the weaker the flow heterogeneity. The Lorenz coefficient is usually regarded as an important evaluation index of flow heterogeneity in a waterflooding reservoir.

3. Dynamic Evolution of Flow Field in Waterflooding Reservoir

In order to explore the dynamic evolution of the flow field in a waterflooding reservoir with strong heterogeneity, a synthetic model with a positive rhythm of permeability is established for oil–water flow simulation. The simulation time is 10 years. There are a total of $30 \times 30 \times 15 = 13,500$ grids, and the grid size is $10 \text{ m} \times 10 \text{ m} \times 5 \text{ m}$. The permeability distribution is shown in Figure 2, the vertical permeability contrast (PC, expressed as the ratio of maximum permeability to minimum permeability) of which is set to 5.0. One injector and four producers are located in the synthetic model. Water is continuously injected at a fixed rate of $240 \text{ m}^3/\text{d}$, and liquid is produced at a fixed rate of $60 \text{ m}^3/\text{d}$. Rock and fluid physical properties of the synthetic model are summarized in Table 1. The oil–water relative permeability curve for two-phase fluid flow is displayed in Figure 3.

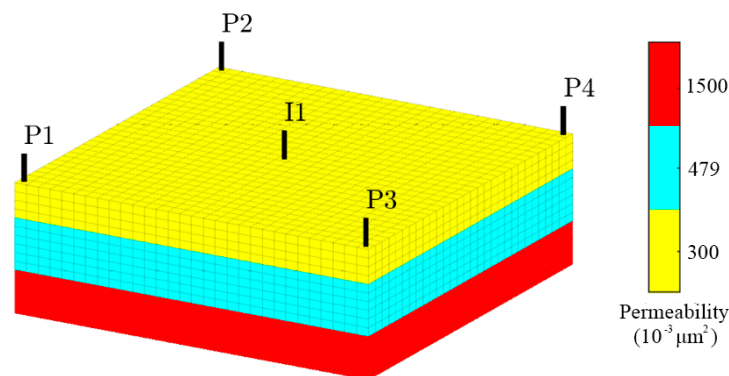
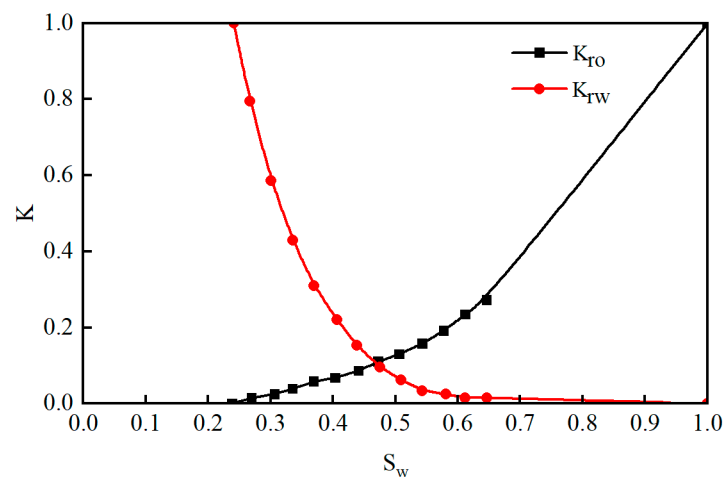


Figure 2. Permeability distribution of the positive–rhythm synthetic model.

Table 1. Rock and fluid physical properties used in the positive-rhythm synthetic model.

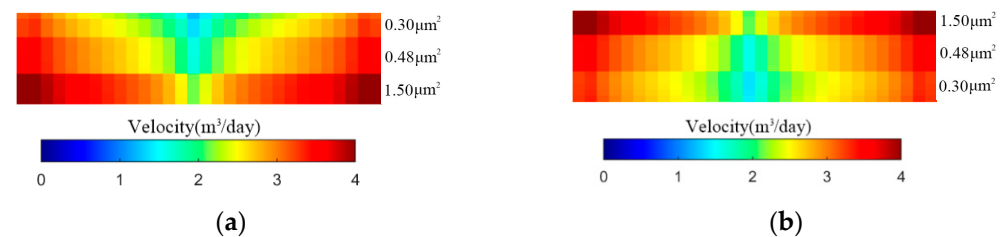
Parameter	Value	Parameter	Value
Initial pressure/(MPa)	8.0	Oil density/(kg·m ³)	866.5
Initial oil saturation	0.7589	Oil viscosity/(mPa·s)	5.0
Porosity	0.235	Oil Volume coefficient/(m ³ /m ³)	1.1
Average permeability, 10 ⁻³ μm ²	760	Oil compressibility/(MPa ⁻¹)	0.002
Permeability contrast	5.0	Water viscosity/(mPa·s)	1.0
Irreducible water saturation	0.2411	Water volume coefficient/(m ³ /m ³)	1.0
Rock compressibility/(MPa ⁻¹)	0.00032	Water compressibility/(MPa ⁻¹)	0.0005
Reservoir rhythm	Positive	Water density/(kg·m ³)	1000

**Figure 3.** Oil–water relative permeability curves used for two-phase flow simulation.

3.1. Effect of Vertical Heterogeneity on Flow Field Evolution

Here, we mainly investigate the effects of rhythm and vertical permeability contrast on the dynamic evolution of the flow field. When the effect of rhythm change is evaluated, the positive-rhythm model and reverse-rhythm model are considered. When the effect of vertical permeability contrast is discussed, three positive-rhythm synthetic models with permeability contrasts of 5.0 (basic model), 15.0, and 30.0 are considered.

Figure 4 shows the fluid velocity profiles of synthetic models with different rhythms. It indicates that the fluid velocity profiles between the basic model and the reverse-rhythm synthetic model are opposite along the vertical direction. For the basic model, injected water flows downward preferentially and bursts along the high-permeability layer, resulting in a higher fluid velocity at the bottom of the positive-rhythm model. Due to lower permeability and higher flow resistance, the fluid velocity profile near the injector in the positive-rhythm model resembles a funnel. For the reverse-rhythm synthetic model, the fluid velocity profile near the injector resembles an inverted funnel.

**Figure 4.** Fluid velocity profile near injector with different rhythm models. (a) Positive rhythm; (b) reverse rhythm.

The effect of the reservoir rhythm on the abundance of the predominant remaining oil is displayed in Figure 5. In the positive-rhythm synthetic model, the abundance of the

predominant remaining oil is distributed in a “U” shape. The area with a higher abundance of predominant remaining oil is located at the top, while the abundance of the predominant remaining oil reserves in the bottom high-permeability layer is almost zero. Due to the remarkable stratification, oil exploitation is severely unbalanced. The vertical degree of producing reserves in the reverse-rhythm synthetic model is more balanced. This is due to the influence of gravity, enabling the injected water to enter the lower layers with low permeability, which effectively inhibits water fingering along the upper high permeability layers. Compared with the reverse-rhythm model, it is much easier to form a large amount of remaining oil in the top region of the positive rhythm model.

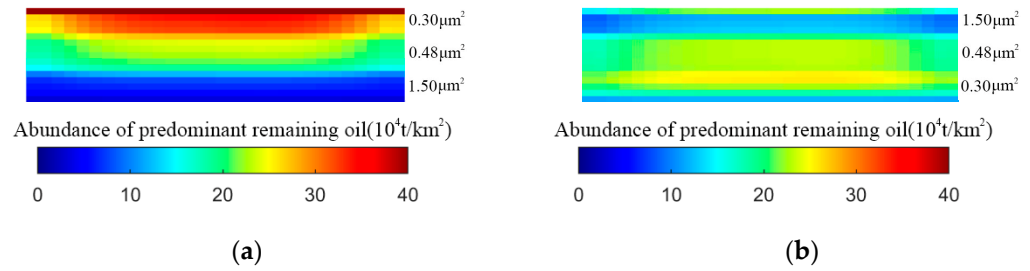


Figure 5. Abundance of predominant remaining oil for synthetic models with different rhythms. (a) Positive rhythm; (b) reverse rhythm.

Figure 6 shows the Lorenz and flow heterogeneity curves when numerical simulation is accomplished. It is referred that there exist two stages of fluid flow from the flow heterogeneity: the unsteady stage and steady stage. The calculated Lorenz coefficient in the steady stage can reflect the degree of dynamic heterogeneity. The larger the Lorenz coefficient, the higher the degree of dynamic heterogeneity. When vertical permeability contrast is identical, the flow heterogeneity curve of the positive-rhythm model shows a similar trend to that of the reverse-rhythm model. The Lorenz coefficient of the positive rhythm model is higher with a value of 0.4018; the Lorenz coefficient of the reverse rhythm model is relatively smaller, 0.3925, indicating that dynamic heterogeneity of the positive rhythm model is stronger even if the same permeability contrast is encountered.

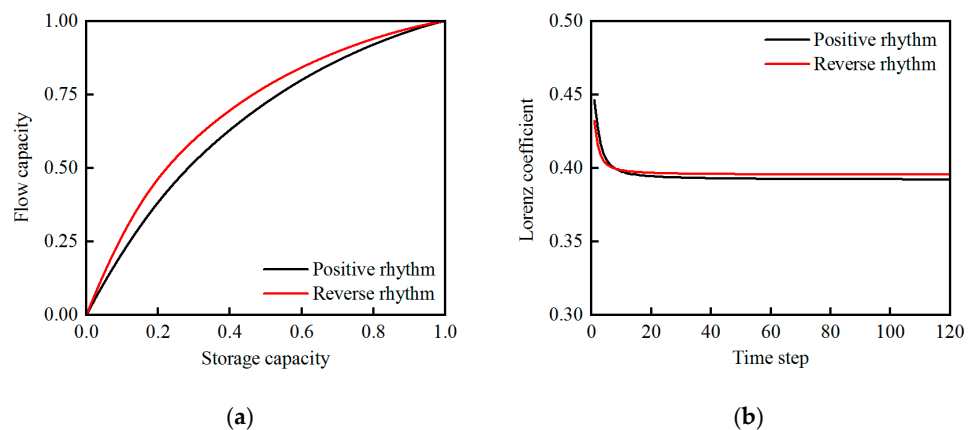


Figure 6. Flow heterogeneity evaluation of synthetic models with different rhythms. (a) Lorenz curve; (b) flow heterogeneity curve.

Figure 7 reflects the effect of vertical permeability contrast on the flow velocity profile near the injector. Affected simultaneously by gravity and pressure drop, injected water prefers to flow downward, causing the velocity to be distributed in a funnel shape. The remaining oil is mainly enriched in the low-permeability layer of the positive-rhythm synthetic model; the larger the permeability contrast, the narrower the funnel shape distribution and the greater the difference in velocity between layers.

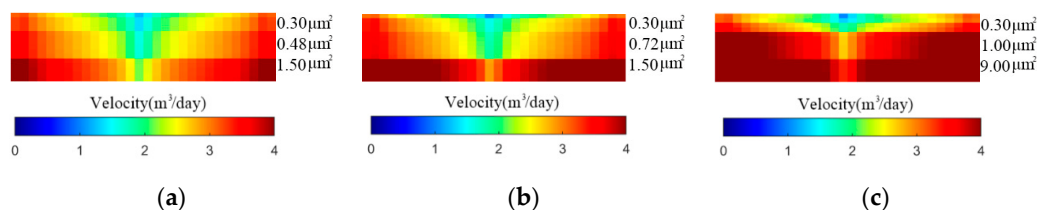


Figure 7. Fluid velocity profiles in the basic model with different permeability contrasts. (a) PC = 5; (b) PC = 15; (c) PC = 30.

Thereafter, the effect of vertical permeability contrast on the abundance of the predominant remaining oil is analyzed. As displayed in Figure 8, when the permeability contrasts are 5.0 and 15.0, respectively, the abundance of predominant remaining oil shows a U-shaped distribution, but it shows a layered distribution when the permeability contrast reaches up to 30. This indicates that, with the increase in vertical permeability contrast, it is more difficult to exploit the remaining oil in low-permeability layers of the positive-rhythm synthetic model.

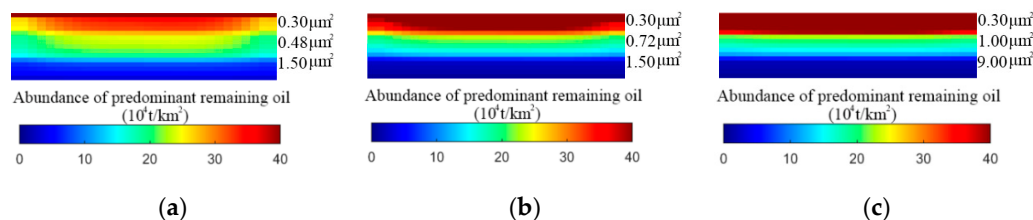


Figure 8. Abundance of predominant remaining oil under different permeability contrasts. (a) PC = 5; (b) PC = 15; (c) PC = 30.

Figure 9 further compares the flow heterogeneity and Lorenz curves of synthetic models with different vertical permeability contrasts when the end of the simulation is achieved. As can be seen from Figure 9, for the positive-rhythm synthetic models, the trend in the unsteady stage of the flow heterogeneity curve is consistent, and the calculated Lorenz coefficients in the steady stage are 0.3918, 0.4204, and 0.5688, respectively. It can be concluded that the reservoir rhythm significantly affects the variation trend in the unsteady stage of the flow heterogeneity curve and has little effect on the Lorenz coefficient in the steady stage. For the positive rhythm synthetic model, the vertical permeability contrast exerts a great impact on the degree of flow heterogeneity. The larger the vertical permeability contrast, the higher the Lorenz coefficient in the steady stage and the stronger the flow heterogeneity.

3.2. Effect of Lateral Heterogeneity on Flow Field Evolution

Lateral heterogeneity refers to the reservoir heterogeneity caused by geometry, scale, continuity, areal variation of porosity, and permeability in the sandbody. To explore the effects of lateral permeability distribution and permeability contrast on the flow field, a single-layer homogeneous synthetic model with a permeability of $0.3 \mu\text{m}^2$ is established. The grid size, injection-production pattern, working scheme, and rock and fluid physical properties are the same as the above-mentioned basic model. Three heterogeneous synthetic models with different permeability distributions were established, as shown in Figure 10. To study the effect of the lateral permeability contrast, the flow fields of single-layer synthetic models with lateral permeability contrasts of 5.0, 20.0, and 30.0 were further analyzed.

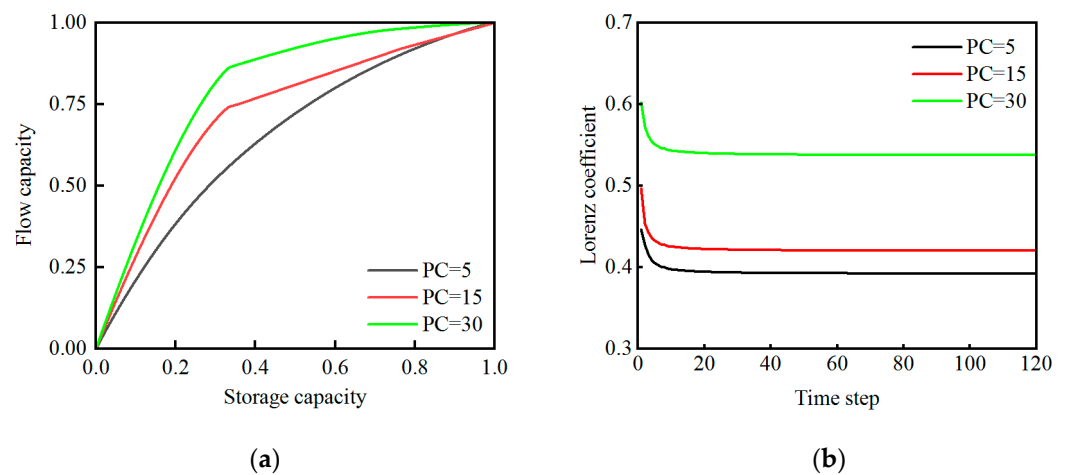


Figure 9. Flow heterogeneity evaluation of synthetic models with different vertical permeability contrasts. (a) Lorenz curve; (b) flow heterogeneity curve.

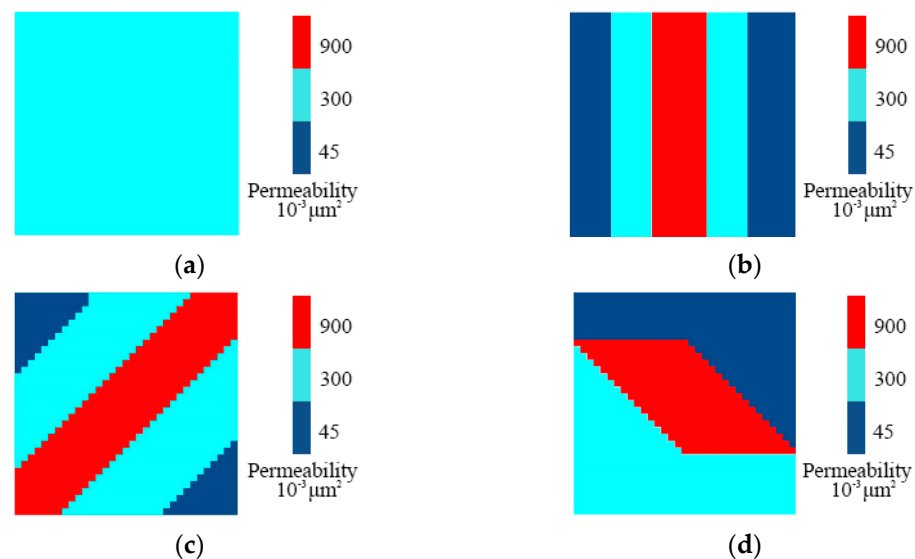


Figure 10. Permeability distribution of four single-layer synthetic models. (a) Homogeneous distribution; (b) vertical distribution; (c) diagonal distribution; (d) block-like distribution.

As shown in Figure 11, the permeability distribution greatly affects the lateral fluid velocity distribution. The high permeability distribution leads to a non-uniform velocity profile, the fingering of the waterfront is severe, and the sweep efficiency is relatively low.

As shown in Figure 12, the influence of the lateral permeability distribution on the abundance of the predominant remaining oil is displayed. It demonstrates that the abundance of predominant remaining oil around the high-permeability distribution and near the injector is lower. This is because of the higher reservoir properties around the high-permeability distribution and the larger mechanical scouring induced by water injection. A dominant flow is formed along the high permeability strip, leading to seriously ineffective water circulation between injector–producer pairs and an unbalanced degree of producing reserves.

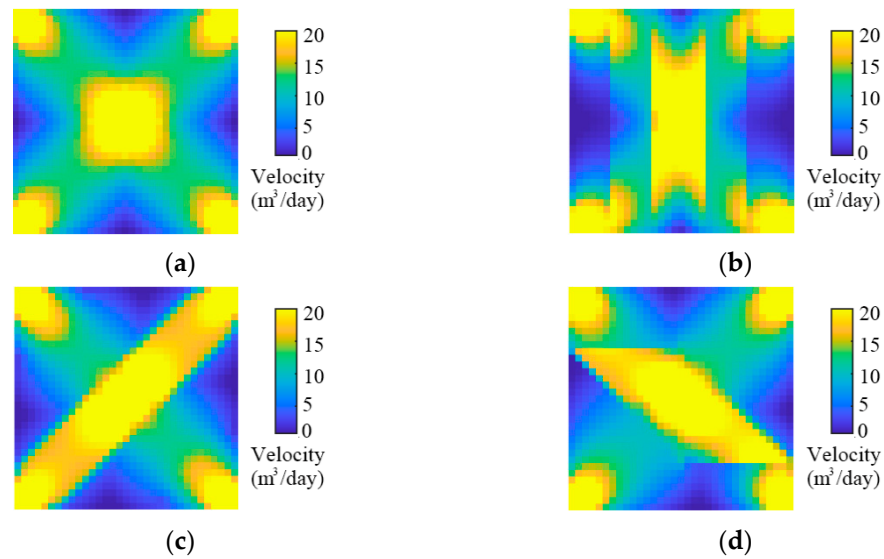


Figure 11. Lateral velocity profiles of synthetic models with different permeability strips. (a) Homogeneous distribution; (b) vertical distribution; (c) diagonal distribution; (d) block-like distribution.

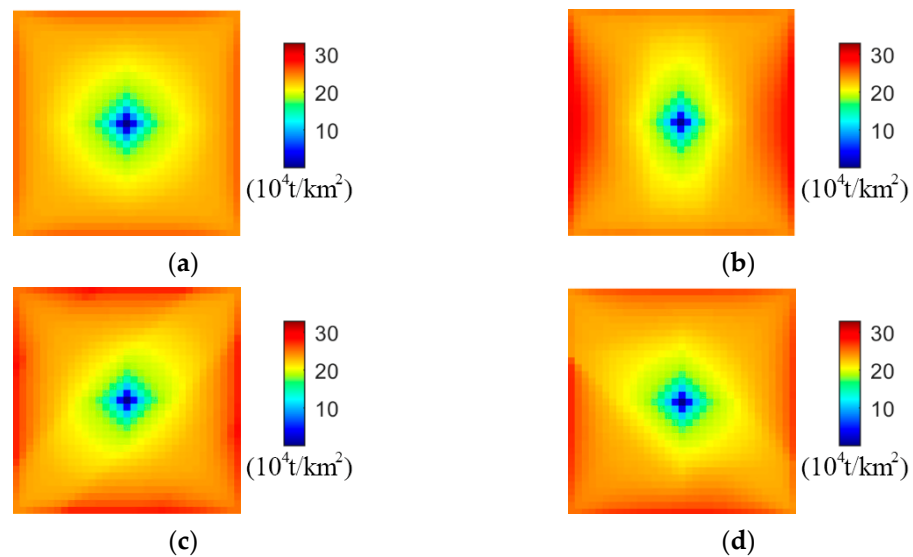


Figure 12. Abundance of predominant remaining oil with different permeability strips. (a) Homogeneous distribution; (b) vertical distribution; (c) diagonal distribution; (d) block-like distribution.

Figure 13 displays the Lorenz and flow heterogeneity curves of the synthetic models with different lateral permeability distributions when the simulation is ended. It indicates that the lateral permeability distribution has a significant effect on the flow heterogeneity curves. The Lorenz coefficients of the synthetic models with a diagonal or block-like permeability strip decrease sharply at the early stage. The initial Lorenz coefficient of the single-layer synthetic model with a diagonal permeability strip is the highest. When the fluid flow reaches a steady state, the calculated Lorenz coefficient is far higher than that of the homogeneous synthetic model, showing the most severe flow heterogeneity.

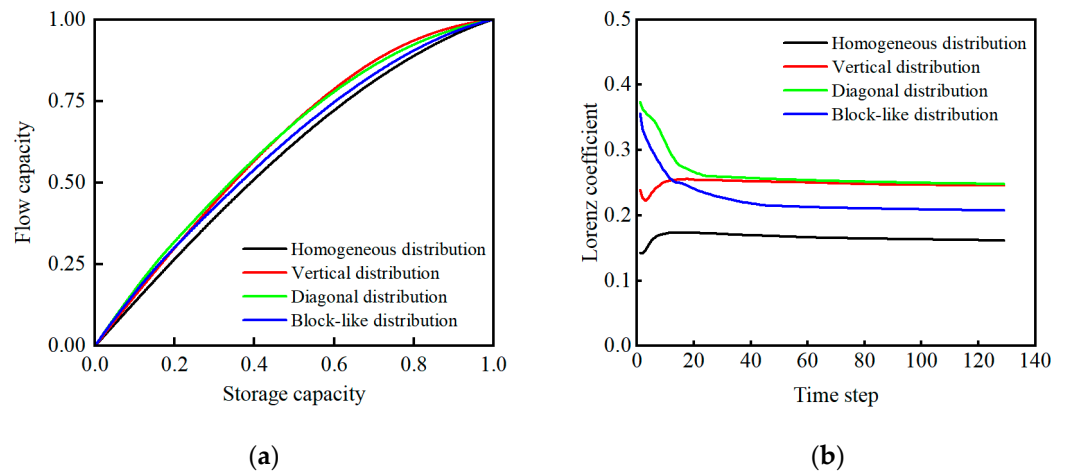


Figure 13. Comparison of flow heterogeneity under different permeability distributions. (a) Lorenz curve; (b) flow heterogeneity curve.

Taking the single-layer synthetic model with a vertical permeability strip as an example, the effect of lateral permeability contrast on fluid velocity is compared. As shown in Figure 14, the larger the lateral permeability contrast, the more obvious the influence of permeability distribution on fluid velocity. Figure 15 shows the Lorenz and flow heterogeneity curves with different lateral permeability contrasts. It can be seen that, for the synthetic model with a vertical permeability strip, the effect of permeability distribution is more significant as the lateral permeability contrast becomes larger. Increasing the permeability contrast will exert a great impact on the Lorenz coefficient. The variation trends of the flow heterogeneity curves under different permeability contrasts are clearly different. When the lateral permeability contrast is higher than 20.0, there is almost no difference in the Lorenz coefficient. It concludes that the permeability distribution has an important influence on the dynamic evolution of the flow field during waterflooding. The larger the lateral permeability contrast is, the greater the influence of permeability distribution is. The flow heterogeneity curve and Lorenz coefficient are synergically affected by the lateral permeability distribution and permeability contrast. When the permeability contrast is large enough, the Lorenz coefficient is more dependent on the permeability distribution.

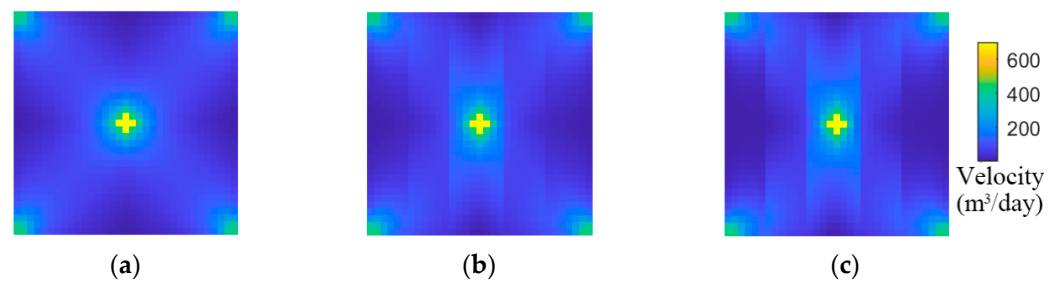


Figure 14. Fluid velocity profiles under different lateral permeability contrasts. (a) PC = 5; (b) PC = 20; (c) PC = 30.

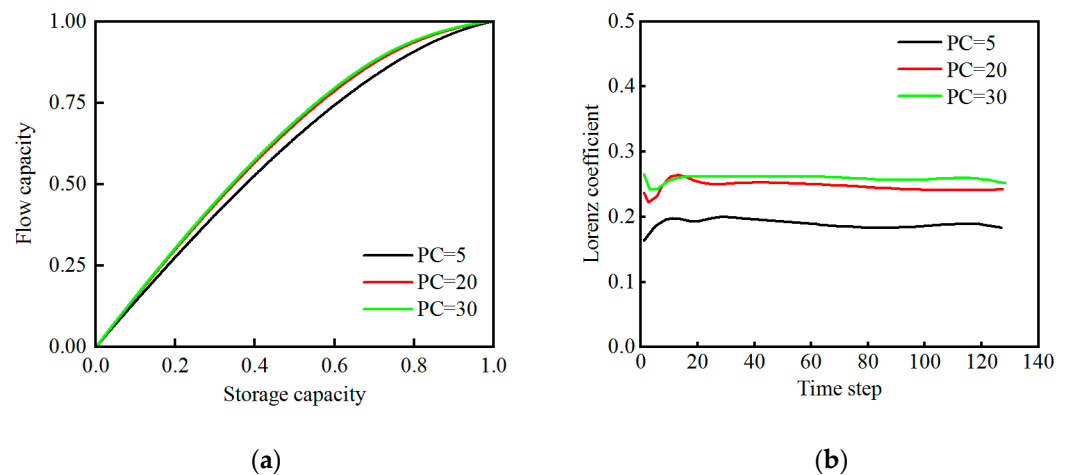


Figure 15. Effect of lateral permeability contrast on the flow heterogeneity. (a) Lorenz curve; (b) flow heterogeneity curve.

4. Dynamic Adjustment of Flow Field

During waterflooding, the liquid production rate needs to be continuously optimized to improve the oil recovery as much as possible. Determining the optimal liquid production rate is a complicated least-square optimization problem. A lot of work has been conducted on intelligent optimization algorithms [33–36]. Great efforts have been made to develop reduced-order models for fast simulation because traditional reservoir production optimization requires a large number of numerical simulations, which are time-consuming and computationally highly demanding [37–41]. Park and Datta-Gupta used a streamline-based model to optimize injection and production schemes by maximizing the reservoir sweep efficiency and balancing the distribution of the time of flight [42]. From the previous studies on the flow field in heterogeneous reservoirs, it is clear that the Lorenz coefficient is a characteristic parameter of the flow field with clear physical meaning, which can easily reflect the difference in flow heterogeneity and the change in flow field caused by reservoir heterogeneity. In this paper, the minimum Lorenz coefficient is taken as the objective function to optimize the liquid production rate of each producer in real time, so as to dynamically adjust the flow field of a heterogeneous reservoir.

To further improve the efficiency of the production optimization, the pore volume weighted by oil saturation is introduced to replace the original pore volume. The modified formula of the Lorenz coefficient is expressed as follows:

$$L_{C,O} = 2 \int_0^1 [F(\Phi) - (\Phi)] S_O d\Phi, \quad (6)$$

The modified formula makes the method applicable to regions with large residual oil enrichment rather than ineffective water circulation. To minimize the Lorenz coefficients during waterflooding in heterogeneous reservoirs, the steepest descent method is adopted in this study, which is one of the most widely used methods for solving unconstrained optimization problems, having the advantage of simple iterations and fewer requirements for prior estimates. Figure 16 shows the optimization procedure of the Lorenz coefficient during waterflooding for a strongly heterogeneous reservoir.

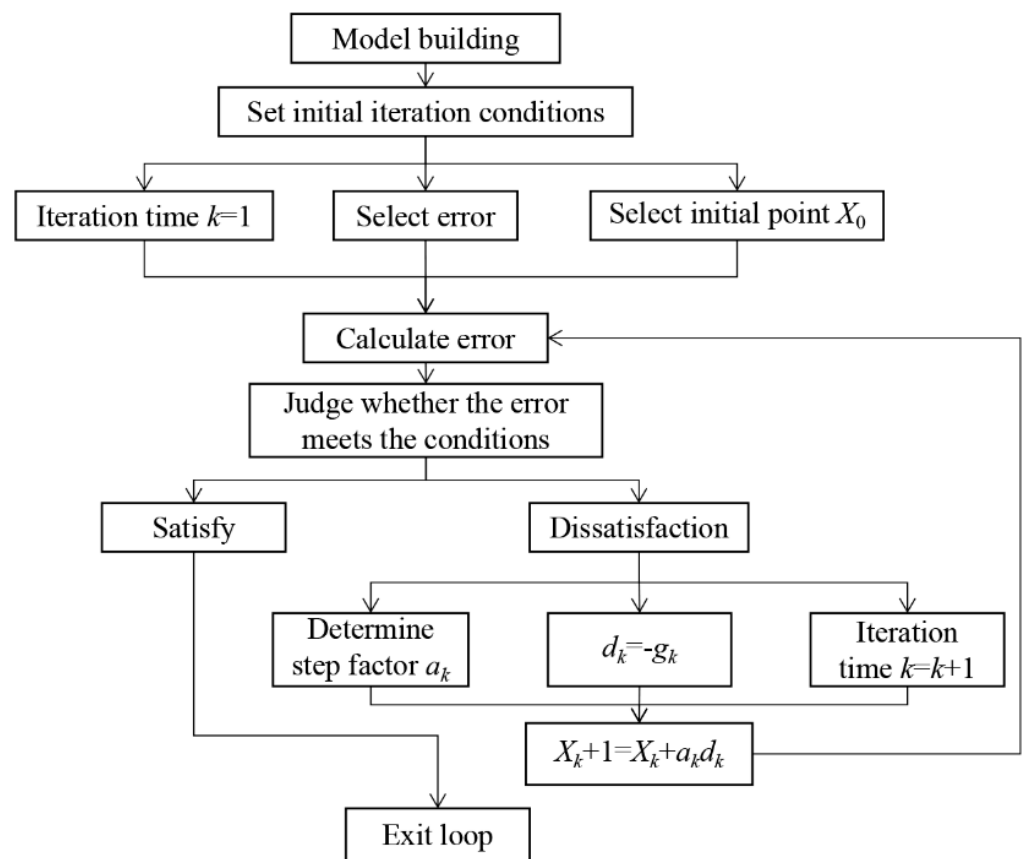


Figure 16. Schematic of Lorenz coefficient optimization in waterflood reservoir.

In the iterative process, the prior estimate is set first, including the initial point X_0 , the iteration error $0 \leq \varepsilon \leq 1$, and the number of iterations $k = 1$. The iteration error under the prior estimate is calculated as follows:

$$g_k = \nabla f(X_k), \quad (7)$$

If the error of two iterations satisfies the condition $\|g_k\| \leq \varepsilon$, the calculation is terminated and the optimal solution will be obtained; if the convergence condition is not satisfied, the negative gradient direction $d_k = -g_k$ is used as the step size of the next iteration, which is the local fastest descent direction of the least-squares objective function. The solution arrived along the negative gradient direction must be better than that of the previous iteration. Then, the step size factor a_k , the formula $X_{k+1} = X_k + a_k d_k$, and the number of iterations $k = k + 1$ are updated. The iteration calculation is repeated until the convergence condition is satisfied to obtain the optimal solution.

Taking the single-layer heterogeneous synthetic model with a block-like permeability strip as an example, the Lorenz coefficient during waterflooding is gradually minimized, and the optimal liquid production rate scheme can be obtained. As shown in Figure 17, all the initial liquid production rates of producers are set at $60 \text{ m}^3/\text{d}$. The optimal liquid production rates are obtained after seven iterations to minimize the Lorenz coefficient. The liquid production rates of producers 1, 2, 3, and 4 are $75.4624 \text{ m}^3/\text{d}$, $45.8296 \text{ m}^3/\text{d}$, $42.4474 \text{ m}^3/\text{d}$, and $76.2605 \text{ m}^3/\text{d}$, respectively.

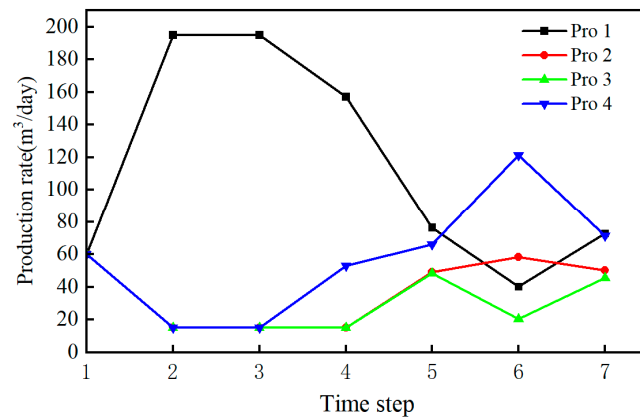


Figure 17. Production optimization in the single-layer model with a block-like permeability strip.

Figure 18 displays the oil recovery and Lorenz curves before and after flow-field adjustment of the single-layer synthetic model with a block-like permeability. The results show that after real-time production optimization, the Lorenz coefficient decreased from 0.1892 to 0.1692, but the performance of enhanced oil recovery merely by dynamic adjustment of flow field is still limited. The oil saturation distribution of the single-layer synthetic model before and after the adjustment of the flow field was further compared, as shown in Figure 19. It indicates that the flow-field adjustment can activate the enriched remaining oil around injector, but the overall remaining oil distribution does not change significantly.

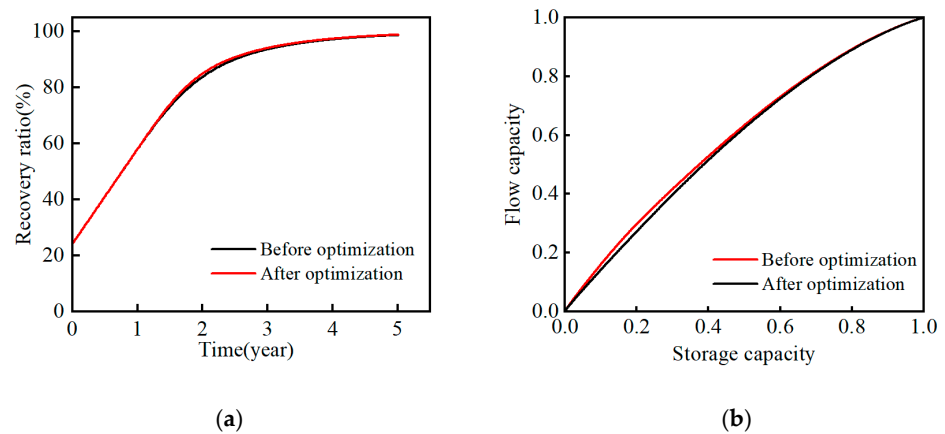


Figure 18. Flow-field adjustment of the single-layer model with a block-like permeability strip. (a) Recovery curve; (b) Lorenz curve.

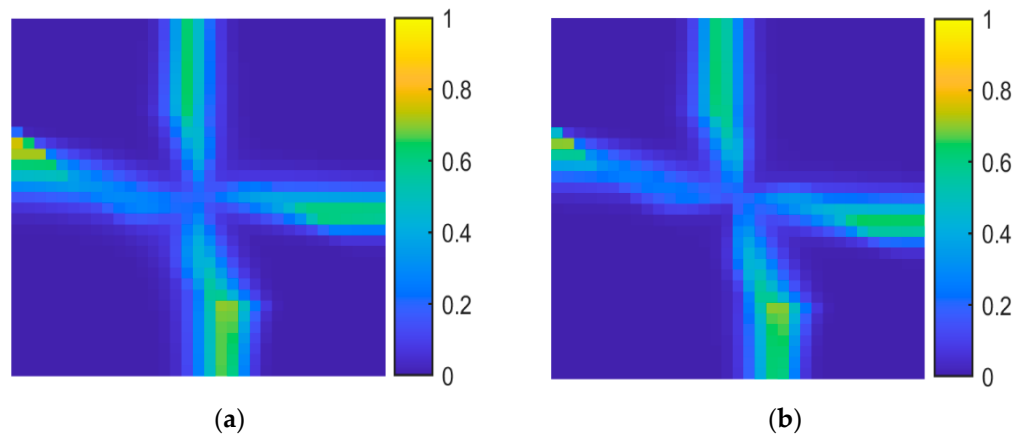


Figure 19. Remaining oil distribution before and after flow-field adjustment in the single-layer synthetic model with a block-like permeability strip. (a) Before adjustment; (b) after adjustment.

5. Case Study

Taking a continental heterogeneous reservoir in China as an example, the proposed method is used to characterize and adjust the reservoir flow field. The reservoir belongs to a fluvial deposit with a cemented sand and mud content of 17.8%, average reservoir thickness of 7.1 m, and porosity of 31%. The reservoir heterogeneity is strong, whose permeability distribution is shown in Figure 20. The lateral permeability contrast is approximately 4.0 and the vertical permeability contrast is up to 30, which shows a typical positive-rhythm distribution. This reservoir has gone through four stages of development—elastic drive, water injection, encryption adjustment, and comprehensive management—and it has entered the extra-high water-cut stage. The water cut reached 96.29%. The lateral and vertical contradiction lead to an uneven production degree and imperfect well pattern, which significantly affects the waterflooding effect.

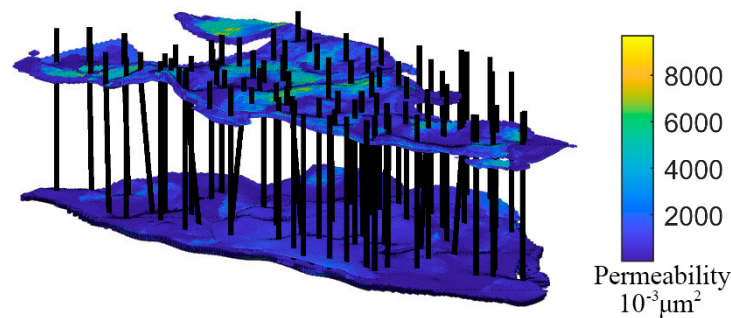


Figure 20. Permeability distribution of a typical continental heterogeneous reservoir.

The Petrel software was used to construct the reservoir simulation model in the corner point grid system. There were a total of $184 \times 57 \times 24 = 2,517,112$ grids, in which 798,956 grids were effective. The grid size in X and Y directions was set to 10 m. In total, 84 producers and 8 injectors were in service. Since it was originally developed in October 1965, the actual cumulative oil production is 171.5×10^4 t. The predicted cumulative oil production is 168.4×10^4 t. The fitting error is 1.8%, indicating that the reservoir simulation model after history matching can reflect the complicated fluid flow dynamics accurately.

Using the proposed method, the Lorenz coefficients of each layer are computed as displayed in Figure 21. It shows that the Lorenz coefficients are between 0.65 and 0.8, in which the 1st and 21st layers show the highest flow heterogeneity. Therefore, we select these two layers to analyze the effect of reservoir heterogeneity on the flow field.

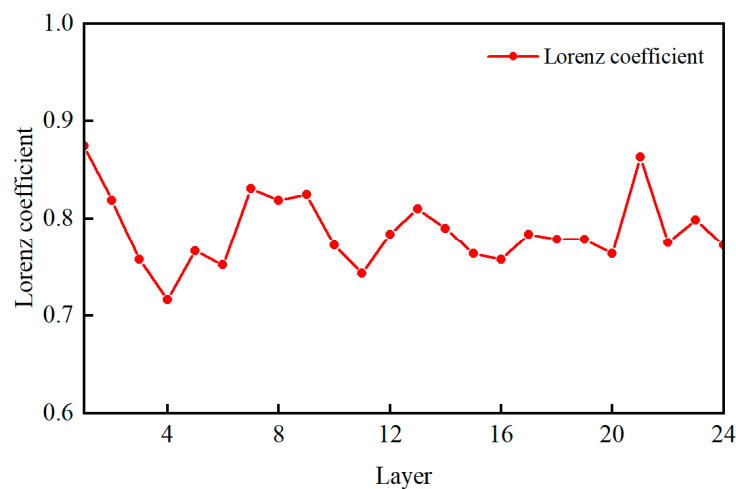


Figure 21. The Lorenz coefficients of each layer in an actual waterflooding reservoir.

The velocity and abundance of predominant remaining oil distribution in the 1st and 21st layers are calculated to characterize the reservoir flow field. The characteristic parameters are normalized and categorized into six groups so as to accurately evaluate the remaining oil potential in different hydrodynamic regions. The classification criterion is summarized in Table 2.

Table 2. Classification of reservoir flow field based on grid attribute mapping.

Type	Flow Velocity	Abundance of Predominant Remaining Oil	Description
1	0–0.4	0–0.33	Both the abundance of predominant remaining oil and the instantaneous flow-field strength are low, indicating effective water injection to displace oil. The existing measures can be maintained to control the evolution of the flow field.
2	0–0.4	0.33–1	The abundance of predominant remaining oil is high, but the instantaneous field strength is low, indicating a relatively weak adjustment ability of well pattern and a locally enriched distribution of remaining oil. More measures should be carried out to enlarge the degree of producing reserves.
3	0.6–1	0.33–1	Both the abundance of predominant remaining oil and the instantaneous field strength are high, indicating effective water injection to displace oil. The existing measures can be maintained to control the evolution of the flow field.
4	0.4–0.6	0.33–1	The abundance of predominant remaining oil is high, and the instantaneous field strength is medium. In order to achieve a good waterflood effect, water injection should be strengthened to improve the degree of producing reserves.
5	0.4–0.6	0–0.33	The abundance of predominant remaining oil is low, and the instantaneous field strength is medium, so the evolution of flow field should be dynamically controlled and adjusted.
6	0.6–1	0–0.33	The abundance of predominant remaining oil is low, but the instantaneous field strength is high, indicating that a satisfactory displacement effect in this area has been achieved.

Figure 22 shows the flow-field-strength distributions in the 1st and 21st layer of the actual heterogeneous reservoir. It indicates that most areas in the 1st layer typically have high abundance of predominant remaining oil and strong instantaneous flow-field strength. Flow-field adjustment is essential to maintain effective water circulation and further tap the remaining oil potential. When the flow field with a high abundance of predominant remaining oil and low instantaneous field strength is dominated, a large amount of remaining oil is still unexploited due to an unreasonable well pattern. The flooding pattern should be improved by perforation to increase the flow-field strength and enlarge the degree of the producing reserves. For the southeast and northwest areas of the 21st layer, a low abundance of predominant remaining oil and high instantaneous flow-field strength can be observed, implying a good waterflooding effect. In addition, a highly scattered distribution with a low abundance of predominant remaining oil and low instantaneous flow-field strength can be found, which indicates that the previous measures controlled the flow-field evolution effectively.

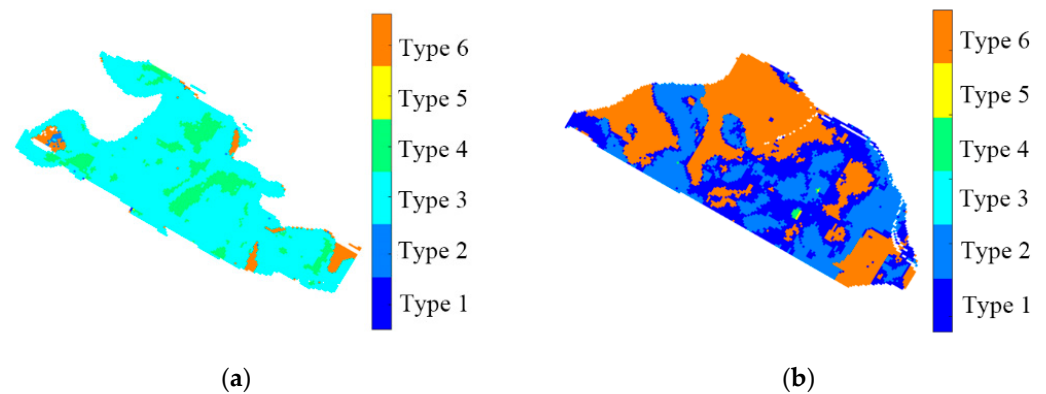


Figure 22. Flow-field strength distribution of certain layers during late stage of waterflooding: (a) 1st layer; (b) 21st layer.

By calculating the time-of-flight distribution, the flow heterogeneity curves of each layer are plotted to obtain the Lorenz coefficients, as displayed in Figure 23. The results show that the Lorenz coefficient rises sharply in the early stage of waterflooding. As water injection continues, it gradually becomes stable. The obvious increase in the Lorenz coefficient in the unsteady stage of the 1st layer and 21st layer is caused by reservoir heterogeneity. There may be a complicated distribution of the permeability strip in the 1st layer and 21st layer, which leads to the distinct fluctuation of the Lorenz coefficient in the stable stage ranging from 0.6 to 0.8. As can be referred from Figure 23, great efforts were made to minimize the Lorenz coefficient as much as possible in order to improve the oil recovery, but the Lorenz coefficient was increased gradually at a later stage, implying that it is of great importance to characterize and adjust the flow field in real time during waterflooding for actual strongly heterogeneous reservoirs.

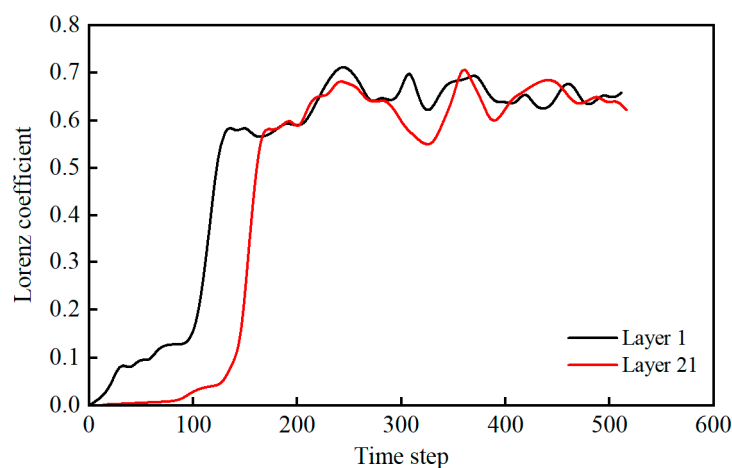


Figure 23. Variation of flow heterogeneity curves during waterflooding.

As can be seen from the above analysis, the flow field with a high abundance of predominant remaining oil and low flow-field strength is widely distributed in the 21st layer, and the flow heterogeneity is high. Dynamic adjustment of the flow field during waterflooding is further carried out. The remaining oil distribution before and after flow-field adjustment in the 21st layer is illustrated in Figure 24. The blue region represents the flow field with a low abundance of predominant remaining oil and high instantaneous flow-field strength, and there is no obvious change in the distribution of remaining oil. However, oil saturation in the area with a high abundance of predominant remaining oil and low instantaneous flow-field strength was decreased slightly.

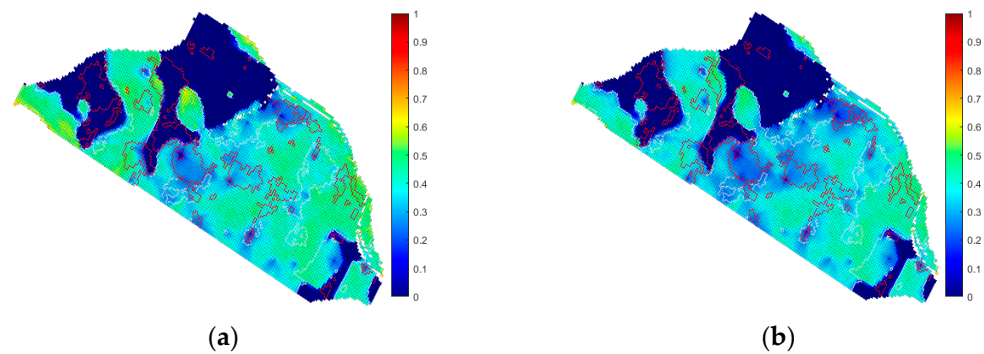


Figure 24. Remaining oil distribution before and after flow-field adjustment in the 21st layer. (a) Before adjustment; (b) after adjustment.

The production performance before and after the adjustment of the flow field in the 21st layer is plotted in Figure 25. The oil recovery ratio and water cut are consistent with each other in the early stage of flow-field adjustment, and an obvious effect of oil increasing and water decreasing in the middle and later stages can be achieved. The optimized injection and production parameters have effectively improved the water flooding performance, but the magnitude of enhanced oil recovery is limited. When the reservoir enters a high or extra-high water-cut period, the injection of chemical agents, e.g., polymer and cross-linked gel, can be treated as a good alternative to further tap the remaining oil.

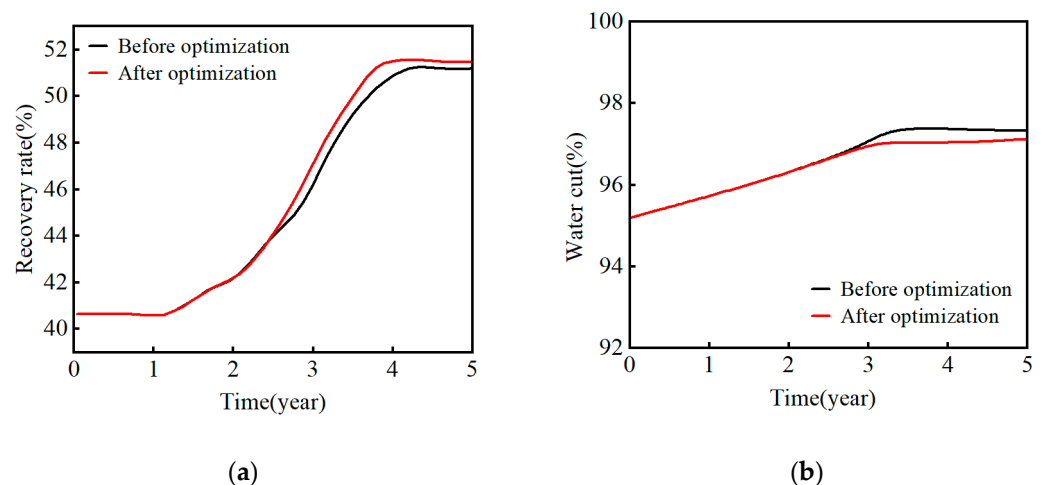


Figure 25. Oil recovery effect before and after flow-field adjustment in the 21st layer. (a) Oil recovery ratio; (b) water cut.

6. Conclusions

For strongly heterogeneous waterflood reservoirs, the flow velocity and abundance of the predominant remaining oil were selected as grid-attribute-mapping-based flow-field properties, and the Lorenz coefficient was utilized to characterize the flow heterogeneity. The influence of reservoir and flow heterogeneity on the dynamic evolution of the flow field during the late stage of waterflooding has been explored. The main conclusions are as follows:

- (1) The shape and variation of the flow field are jointly affected by the reservoir rhythm, vertical permeability contrast, and lateral permeability distribution. The larger the permeability contrast, the greater the effect of the lateral permeability distribution.
- (2) For vertical heterogeneity, the permeability contrast exerts a significant impact on the Lorenz coefficient; when the permeability contrast increases by 6 times, the Lorenz coefficient increases by about 1.5 times. For lateral heterogeneity, when the

- permeability contrast is large, the Lorentz coefficient strongly depends on the lateral permeability distribution.
- (3) To realize the flow-field adjustment, a dynamic adjustment method for the flow field in a strongly heterogeneous reservoir is established with the objective function of minimizing the Lorentz coefficient. Mechanistic modeling shows that the method can effectively improve the waterflooding development effect, but the magnitude of improving oil recovery is usually limited.
 - (4) Using the proposed method, the flow field of a continental heterogeneous reservoir is characterized and adjusted. The flow-field areas with a high abundance of predominant remaining oil and low flow-field strength have been effectively exploited. After the flow-field adjustment is achieved by real-time optimizing the production scheme, a better effect of oil increasing and water decreasing is achieved.

Author Contributions: Conceptualization, D.W., F.L., G.L., S.H. and K.S.; methodology, D.W.; software, F.L.; validation, G.L., S.H. and K.S.; formal analysis, D.W.; investigation, F.L.; resources, G.L.; data curation, S.H.; writing—original draft preparation, K.S.; writing—review and editing, D.W.; visualization, F.L.; supervision, G.L.; funding acquisition, S.H. and J.Z. All authors have read and agreed to the published version of the manuscript.

Funding: This research was funded by the National Natural Science Foundation of China (Grant No. 51834005 and 52174043), Science Foundation of China University of Petroleum, Beijing (No.2462020BJRC006), Prospective and Fundamental Science and Technology Project, PetroChina (Grant No. 2021DJ1002, 2022KT0906 and 2021DJ1502).

Data Availability Statement: The data presented in this study are available on request from the corresponding author.

Acknowledgments: The authors thank the anonymous reviewers for their insightful comments, which have greatly improved the quality of this paper.

Conflicts of Interest: The author declares no conflict of interest.

References

1. Anderson, W.G. Wettability Literature Survey Part 5: The Effects of Wettability on Relative Permeability. *J. Pet. Technol.* **1987**, *39*, 1453–1468. [[CrossRef](#)]
2. Jiang, R.; Qiao, X.; Teng, W.; Xu, J.; Sun, Z.; Xie, L. Impact of physical properties time variation on waterflooding reservoir development. *Fault-Block Oil Gas Field* **2016**, *23*, 768–771. [[CrossRef](#)]
3. Spooner, V.E.; Geiger, S.; Arnold, D. Dual-Porosity Flow Diagnostics for Spontaneous Imbibition in Naturally Fractured Reservoirs. *Water Resour. Res.* **2021**, *57*, e2020WR027775. [[CrossRef](#)]
4. Spooner, V.; Geiger, S.; Arnold, D. Flow diagnostics for naturally fractured reservoirs. *Pet. Geosci.* **2019**, *25*, 490–500. [[CrossRef](#)]
5. Spooner, V.; Geiger, S.; Arnold, D. Ranking Fractured Reservoir Models Using Flow Diagnostics. In Proceedings of the SPE Reservoir Simulation Conference, Galveston, TX, USA, 10–11 April 2019. [[CrossRef](#)]
6. Willis, B.J.; Sech, R.P. Quantifying impacts of fluvial intra-channel-belt heterogeneity on reservoir behaviour. In *Fluvial Meanders and Their Sedimentary Products in the Rock Record*; Wiley: New York, NY, USA, 2018; pp. 543–572. [[CrossRef](#)]
7. Baker, R.; Kuppe, F.; Chugh, S.; Bora, R.; Stojanovic, S.; Batycky, R. Full-Field Modeling Using Streamline-Based Simulation: Four Case Studies. *SPE Reserv. Eval. Eng.* **2002**, *5*, 126–134. [[CrossRef](#)]
8. Datta-Gupta, A. Streamline Simulation: A Technology Update (includes associated papers 71204 and 71764). *J. Pet. Technol.* **2000**, *52*, 68–84. [[CrossRef](#)]
9. Datta-Gupta, A.; King, M.J. *Streamline Simulation: Theory and Practice*; Society of Petroleum Engineers: Richardson, TX, USA, 2007. [[CrossRef](#)]
10. Thiele, M.R.; Batycky, R.P. Using Streamline-Derived Injection Efficiencies for Improved Waterflood Management. *SPE Reserv. Eval. Eng.* **2006**, *9*, 187–196. [[CrossRef](#)]
11. Batycky, R.P.; Thiele, M.R. Technology Update: Mature Flood Surveillance Using Streamlines. *J. Pet. Technol.* **2016**, *68*, 22–25. [[CrossRef](#)]
12. Chen, H.; Park, J.; Datta-Gupta, A.; Shekhar, S.; Grover, K.; Das, J.; Shankar, V.; Kumar, M.S.; Chitale, A. Improving Polymerflood Performance Via Streamline-Based Rate Optimization: Mangala Field, India. In Proceedings of the SPE Improved Oil Recovery Conference, Virtual, 31 August–4 September 2020. [[CrossRef](#)]
13. Zhang, N.; Cao, J.; James, L.A.; Johansen, T.E. High-order streamline simulation and macro-scale visualization experimental studies on waterflooding under given pressure boundaries. *J. Pet. Sci. Eng.* **2021**, *203*, 108617. [[CrossRef](#)]

14. Jia, H.; Deng, L. Water flooding flowing area identification for oil reservoirs based on the method of streamline clustering artificial intelligence. *Pet. Explor. Dev.* **2018**, *45*, 328–335. [[CrossRef](#)]
15. Tanaka, S.; Onishi, T.; Kam, D.; Dehghani, K.; Wen, X.-H. Application of Combined Streamline Based Reduced-Physics Surrogate and Response Surface Method for Field Development Optimization. In Proceedings of the International Petroleum Technology Conference, Dhahran, Kingdom of Saudi Arabia, 13–15 January 2020. [[CrossRef](#)]
16. Natvig, J.R.; Lie, K.A.; Eikemo, B. Fast solvers for flow in porous media based on discontinuous Galerkin methods and optimal reordering. In Proceedings of the XVI International Conference on Computational Methods in Water Resources, Copenhagen, Denmark, 18–22 June 2006. [[CrossRef](#)]
17. Natvig, J.R.; Lie, K.-A. Fast computation of multiphase flow in porous media by implicit discontinuous Galerkin schemes with optimal ordering of elements. *J. Comput. Phys.* **2008**, *227*, 10108–10124. [[CrossRef](#)]
18. Mfoubat, H.R.N.B.; Zaky, E.I. Optimization of waterflooding performance by using finite volume-based flow diagnostics simulation. *J. Pet. Explor. Prod. Technol.* **2019**, *10*, 943–957. [[CrossRef](#)]
19. Borregales, M.; Møyner, O.; Krogstad, S.; Lie, K. Data-Driven Models Based on Flow Diagnostics. In Proceedings of the 16th European Conference on the Mathematics of Oil Recovery, Barcelona, Spain, 3–6 September 2018. [[CrossRef](#)]
20. Shahvali, M.; Mallison, B.; Wei, K.; Gross, H. An Alternative to Streamlines for Flow Diagnostics on Structured and Unstructured Grids. *SPE J.* **2012**, *17*, 768–778. [[CrossRef](#)]
21. Møyner, O.; Krogstad, S.; Lie, K.-A. The Application of Flow Diagnostics for Reservoir Management. *SPE J.* **2014**, *20*, 306–323. [[CrossRef](#)]
22. Zhang, Z.; Geiger, S.; Rood, M.; Jacquemyn, C.; Jackson, M.; Hampson, G.; De Carvalho, F.M.; Silva, C.C.M.M.; Silva, J.M.; Sousa, M.C. Flow Diagnostics on Fully Unstructured Grids. In Proceedings of the SPE Reservoir Simulation Conference, Montgomery, TX, USA, 20–22 February 2017. [[CrossRef](#)]
23. Rasmussen, A.; Lie, K. Discretization of Flow Diagnostics on Stratigraphic and Unstructured Grids. In Proceedings of the ECMOR XIV-14th European Conference on the Mathematics of Oil Recovery, Catania, Italy, 8–11 September 2014. [[CrossRef](#)]
24. Zhang, Q.; Jiang, R.; Jiang, P.; Yao, Z.; Wang, Y.; Peng, W. Establishment and application of oil reservoir flow-field evaluating system. *Pet. Geol. Oilfield Dev. Daqing* **2014**, *33*, 86–89. [[CrossRef](#)]
25. Jiang, R.; Zhang, W.; Zhao, P.; Jiang, Y.; Cai, M.; Tao, Z.; Zhao, M.; Ni, T.; Xu, J.; Cui, Y.; et al. Characterization of the reservoir property time-variation based on ‘surface flux’ and simulator development. *Fuel* **2018**, *234*, 924–933. [[CrossRef](#)]
26. Geng, Z.L.; Jiang, H.Q.; Chen, M.F. A New Method for Quantitative Characterization on Remaining Oil Potential in High Water Cut Oil Reservoirs. *Pet. Geol. Recovery Effic.* **2007**, *14*, 100. [[CrossRef](#)]
27. Krogstad, S.; Lie, K.-A.; Nilsen, H.M.; Berg, C.F.; Kippe, V. Efficient flow diagnostics proxies for polymer flooding. *Comput. Geosci.* **2017**, *21*, 1203–1218. [[CrossRef](#)]
28. Kulkarni, K.N.; Datta-Gupta, A.; Vasco, D. A Streamline Approach for Integrating Transient Pressure Data Into High-Resolution Reservoir Models. *SPE J.* **2001**, *6*, 273–282. [[CrossRef](#)]
29. Vasco, D.; Keers, H.; Karasaki, K. Estimation of reservoir properties using transient pressure data: An asymptotic approach. *Water Resour. Res.* **2000**, *36*, 3447–3465. [[CrossRef](#)]
30. Natvig, J.R.; Lie, K.; Eikemo, B.; Berre, I. An efficient discontinuous Galerkin method for advective transport in porous media. *Adv. Water Resour.* **2007**, *30*, 2424–2438. [[CrossRef](#)]
31. Lake, L.W. Enhanced Oil Recovery. 1989. Available online: <https://www.osti.gov/biblio/5112525> (accessed on 10 January 2022).
32. Shook, G.M.; Mitchell, K.M. A Robust Measure of Heterogeneity for Ranking Earth Models: The F-PHI Curve and Dynamic Lorenz Coefficient. In Proceedings of the SPE Annual Technical Conference and Exhibition, New Orleans, Louisiana, 4–7 October 2009. [[CrossRef](#)]
33. Brouwer, D.R.; Jansen, J.D. Dynamic Optimization of Water Flooding with Smart Wells Using Optimal Control Theory. In Proceedings of the European Petroleum Conference, Aberdeen, UK, 29–31 October 2002. [[CrossRef](#)]
34. Lorentzen, R.J.; Berg, A.M.; Nævdal, G.; Vefring, E.H. A New Approach for Dynamic Optimization of Waterflooding Problems. In Proceedings of the Intelligent Energy Conference and Exhibition, Amsterdam, The Netherlands, 11–13 April 2006. [[CrossRef](#)]
35. Ma, K.; Li, A.; Guo, S.; Pang, J.; Xue, Y.; Zhou, Z. Techniques for improving the water-flooding of oil fields during the high water-cut stage. *Oil Gas Sci. Technol.–Rev. D’ifp Energ. Nouv.* **2019**, *74*, 69. [[CrossRef](#)]
36. de Brito, D.U.; Durlofsky, L.J. Well control optimization using a two-step surrogate treatment. *J. Pet. Sci. Eng.* **2019**, *187*, 106565. [[CrossRef](#)]
37. Sudaryanto, B.; Yortsos, Y.C. Optimization of fluid front dynamics in porous media using rate control. I. Equal mobility fluids. *Phys. Fluids* **2000**, *12*, 1656–1670. [[CrossRef](#)]
38. Yeten, B.; Brouwer, D.; Durlofsky, L.; Aziz, K. Decision analysis under uncertainty for smart well deployment. *J. Pet. Sci. Eng.* **2004**, *44*, 175–191. [[CrossRef](#)]
39. Josset, L.; Ginsbourger, D.; Lunati, I. Functional error modeling for uncertainty quantification in hydrogeology. *Water Resour. Res.* **2015**, *51*, 1050–1068. [[CrossRef](#)]
40. Oladyshkin, S.; Class, H.; Helmig, R.; Nowak, W. An integrative approach to robust design and probabilistic risk assessment for CO₂ storage in geological formations. *Comput. Geosci.* **2011**, *15*, 565–577. [[CrossRef](#)]

41. Schulte, D.O.; Arnold, D.; Geiger, S.; Demyanov, V.; Sass, I. Multi-objective optimization under uncertainty of geothermal reservoirs using experimental design-based proxy models. *Geothermics* **2020**, *86*, 101792. [[CrossRef](#)]
42. Park, H.-Y.; Datta-Gupta, A. Reservoir Management Using Streamline-Based Flood Efficiency Maps and Application to Rate Optimization. In Proceedings of the SPE Western North American Region Meeting, Anchorage, AK, USA, 7–11 May 2011. [[CrossRef](#)]

Disclaimer/Publisher’s Note: The statements, opinions and data contained in all publications are solely those of the individual author(s) and contributor(s) and not of MDPI and/or the editor(s). MDPI and/or the editor(s) disclaim responsibility for any injury to people or property resulting from any ideas, methods, instructions or products referred to in the content.